Journal of Molecular Graphics and Modelling 42 (2013) 104–114

Contents lists available at SciVerse ScienceDirect

Journal of Molecular Graphics and Modelling

journal homepage: www.elsevier.com/locate/JMGM

Elaborate ligand-based modeling reveal new migration inhibitory factor inhibitors

Mahmoud A. Al-Sha'er[a], Sonya VanPatten[b], Yousef Al-Abed[b], Mutasem O. Taha[c,*]

[a] Faculty of Pharmacy, Zarqa University, Zarqa, 13132, Jordan
[b] Center for Molecular Innovation, The Feinstein Institute for Medical Research, 350 Community Drive, Manhasset, NY, 11030, United States
[c] Department of Pharmaceutical Sciences, Faculty of Pharmacy, University of Jordan, Amman, Jordan

ARTICLE INFO

Article history:
Accepted 16 March 2013
Available online 28 March 2013

Keywords:
Migration inhibitory factor
Pharmacophore modeling
Quantitative structure–activity relationship
In silico screening

ABSTRACT

Recent research suggested the involvement of migration inhibitor factor (MIF) in cancer and inflammatory diseases, which prompted several attempts to develop new MIF inhibitors. Accordingly, we investigated the pharmacophoric space of 79 MIF inhibitors using seven diverse subsets of inhibitors to identify plausible binding hypotheses (pharmacophores). Subsequently, we implemented genetic algorithm and multiple linear regression analysis to select optimal combination of pharmacophores and physicochemical descriptors capable of explaining bioactivity variation within the training compounds (QSAR model, $r_{63}=0.62$, $F=42.8$, $r^2_{LOO}=0.721$, r^2_{PRESS} against 16 external test inhibitors = 0.58). Two orthogonal pharmacophores appeared in the optimal QSAR model suggestive of at least two binding modes available to ligands inside MIF binding pocket. Subsequent validation using receiver operating characteristic (ROC) curves analysis established the validity of these two pharmacophores. We employed these pharmacophoric models and associated QSAR equation to screen the National Cancer Institute (NCI) list of compounds. Eight compounds gave >50% inhibition at 100 μM. Two molecules illustrated >75% inhibition at 10 μM.

1. Introduction

1.1. Macrophage migration inhibitory factor

Macrophage migration inhibitory factor (MIF) functions as a pleiotropic protein, participating in inflammatory and immune responses [1]. MIF was originally discovered as a lymphokine involved in delayed hypersensitivity and various macrophage functions, including phagocytosis, spreading, and tumoricidal activity. Recently, MIF was reevaluated as a proinflammatory cytokine and pituitary-derived hormone potentiating endotoxemia [2,3]. This protein is ubiquitously expressed in various organs, such as the brain and kidney. Among cytokines, MIF is unique in terms of its abundant expression and storage within the cytoplasm and, further, for its counteraction against glucocorticoids [4,5]. MIF has unexpectedly been found to convert D-dopachrome, an enantiomer of naturally occurring L-dopachrome, to 5,6-dihydroxyindole [6]. However, its physiologic significance remains to be completely elucidated. It was demonstrated that anti-MIF antibodies effectively suppress tumor growth and tumor-associated angiogenesis, suggesting that MIF is involved not only in inflammatory and immune responses but also in tumor cell growth [7,8]. At present, MIF cannot be clearly categorized as a cytokine, hormone, or enzyme, however, it has roles in the immune system, cell growth, tumorigenesis and wound repair, in addition to potential functions in various pathophysiologic states [9,64].

The main focus of recent efforts towards the development of new MIF inhibitors concentrate on structure-based ligand design [10–13] and high throughput screening [14], with few ligand-based examples [15,16]. To date, several MIF X-ray complexes are documented in the Protein Data Bank (e.g., PDB codes: 1LJT, 2OOW, 2OOZ, 2HOF, 3IJG, 3IJJ, 3JSF, 3JSG, 3L5P, 3L5R, 3L5S, 3L5T, 3L5U). However, crystallographic structures might be limited by inadequate resolution [17,62] and crystallization-related artifacts of the ligand–protein complex [18–20]. Furthermore, structure-based drug discovery techniques tend to ignore structural heterogeneity related to protein anisotropic motion and discrete conformational substates [21]. Nevertheless, structure-based modeling has been reported to successfully allow the discovery of new micromolar MIF inhibitors [63].

The continuous pursue for new MIF inhibitors and lack of satisfactory ligand-based computer-aided drug discovery efforts for new MIF inhibitors, combined with the potential weaknesses of structure-based design and the significant flexibility observed for MIF [22,65,66], prompted us to explore the possibility of developing ligand-based binding pharmacophore(s) integrated within

* Corresponding author. Tel.: +962 65355000x23305; fax: +962 65339649.
E-mail address: mutasem@ju.edu.jo (M.O. Taha).

1093-3263/$ – see front matter © 2013 Elsevier Inc. All rights reserved.
http://dx.doi.org/10.1016/j.jmgm.2013.03.003

self-consistent QSAR model. This approach avoids depending on structure-based techniques; furthermore, the binding model(s) can be used as 3D search query to discover new MIF inhibitory scaffolds. We previously reported the use of this innovative approach towards the discovery of new inhibitory leads against glycogen synthase kinase-3β [23], bacterial MurF [24], protein tyrosine phosphatase [25], DPP IV [26], hormone sensitive lipase [27], β-secretase [28], influenza neuraminidase [29], cholesteryl ester transfer protein [30], cyclin dependent kinase inhibitors (CDK1) [31], and heat shock protein 90 (Hsp90) [32].

2. Experimental

2.1. Molecular modeling

Pharmacophore and QSAR modeling studies were performed using CATALYST (HYPOGEN module) [33] and CERIUS2 software suites from Accelrys Inc. (San Diego, California, www.accelrys.com) installed on a Silicon Graphics Octane2 desktop workstation equipped with a dual 600 MHz MIPS R14000 processor (1.0 GB RAM) running the Irix 6.5 operating system. Structure drawing was performed employing ChemDraw Ultra 7.0(Cambridge Soft Corp. (http://www.cambridgesoft.com, USA) installed on a Pentium 4 PC.

2.1.1. Data set and conformational analysis

The structures of 79 MIF inhibitors (**1**–**79**, Table A under Supplementary Material) were collected from recently published literature [34–36,60,61]. Although the in vitro bioactivities of the collected inhibitors were gathered from three separate articles they were determined employing similar bioassay methodologies. The in vitro bioactivities of the inhibitors are expressed as the concentration of the test compound that inhibited MIF activity by 50% (IC_{50}). However, to alleviate any bioactivity discrepancies due to minor differences in the bioassay procedures, i.e., among literature sources, and to allow appropriate QSAR analysis, we converted and normalized the bioactivities of all inhibitors into K_i format. Therefore, IC_{50} values were converted into K_i values employing the Cheng–Prusoff equation [37]:

$$K_i = \frac{IC_{50}}{1 + (S/K_m)} \quad (1)$$

where K_m is the Michaelis constant for a particular enzyme (equals 200 μM for MIF [34]) and S is the substrate concentration reported in the particular literature source. The logarithm of calculated K_i (μM) values were used in the three-dimensional quantitative structure activity analysis (3D-QSAR), thus correlating the data linear to the free energy change. In few cases where the K_i values of some compounds were expressed as being higher than 200 μM (12 compounds), we assumed that their IC_{50} values to be equal to 1000 μM (i.e. to all 4 logarithmic cycles away from the most potent inhibitor). These assumptions are necessary to allow pharmacophore modeling, statistical correlation and QSAR analysis. Moreover, such assumptions should have minimal impact on the pharmacophore modeling process as inactive compounds are used to filter out poor pharmacophores (in the substractive phase of the CATALYST algorithm) regardless to their actual bioactivities [33]. Moreover, the logarithmic transformation of IC_{50} values should minimize any potential errors resulting from such assumptions. We successfully implemented such approximations in some of our earlier pharmacophore and QSAR modeling projects [24,27,28,30].

ChemDraw Ultra was used to sketch the two-dimensional (2D) chemical structures of the collected inhibitors. The structures were saved in MDL-molfile format and were subsequently imported into CATALYST, converted into corresponding standard 3D structures and energy minimized to the closest local minimum using CHARMm force field (1000 steps of steepest descent with a RMS gradient tolerance of 3, followed by conjugate gradient minimization of a maximum of 200 steps at and termination cutoff of 0.1 kcal/(mol Å)). The resulting 3D structures were utilized as starting conformers for CATALYST conformational analysis.

The conformational space of each collected inhibitor (**1**–**79**, Table A under supplementary material) was explored using CHARMm force field [33], such that a conformational ensemble was generated for each compound with an energy threshold of 20 kcal/mol from the local minimized structure with a maximum limit of 250 conformers per molecule [33,53].

2.1.2. Generation and assessment of binding hypotheses

All 79 molecules with their associated conformational models were grouped into a spreadsheet. The biological data of the inhibitors were reported with uncertainty = 3, which means that the actual bioactivity of an inhibitor is assumed to be situated somewhere in an interval ranging from one-third to three-times the reported bioactivity value of that inhibitor [38,39]. Subsequently, seven structurally diverse training subsets were carefully selected: subsets **I**, **II**, **III**, **IV**, **V**, **VI** and **VII** shown in table B under Supplementary Materials. Typically, CATALYST requires informative training sets that include at least 16 compounds of evenly spread bioactivities over at least 3.5 logarithmic cycles. Shorter training lists can lead to chance correlation and faulty models.

The selected training sets were utilized to conduct 56 modeling runs to explore the pharmacophoric space of MIF inhibitors. Table C under Supplementary Materials shows the training subsets and different parameters implemented for each pharmacophore exploration run. The exploration process included altering interfeature spacing parameter (100 and 300 picometers) and the maximum number of allowed features in the resulting pharmacophore hypotheses.

Pharmacophore modeling employing CATALYST proceeds through three successive phases: the constructive phase, subtractive phase and optimization phase (see CATALYST Modeling Algorithm under Section **SM-1** in Supplementary Materials) [33,38–42]. In the optimization phase, CATALYST attempts to minimize a cost function for each hypotheses consisting of three terms: Weight cost, Error cost and Configuration cost (see CATALYST Cost Analysis in Assessment of Generated Binding Hypotheses under Section **SM-2** in Supplementary Materials).

CATALYST-HYPOGEN cross-validates the resulting optimal pharmacophores using the Cat-Scramble program implemented in CATALYST. This validation procedure is based on Fischer's randomization test [44]. In this validation test; we selected a 95% confidence level, which instruct CATALYST to generate 19 random spreadsheets. Subsequently, CATALYST-HYPOGEN is challenged to use these scramble spreadsheets to generate hypotheses using the same features and parameters employed in generating the initial unscrambled hypotheses. Success in generating pharmacophores of comparable cost criteria to those produced by the original unscrambled data reduces the confidence in the training compounds and the unscrambled original pharmacophore models [33,43,44]. Based on Fischer randomization criteria; only 403 pharmacophores exceeded the 85% significance threshold for subsequent processing. Table D under Supplementary Materials shows different cost criteria and significance levels of representative pharmacophoric hypotheses (see pharmacophore clustering under Section 2.1.3).

2.1.3. QSAR modeling

The successful pharmacophore models (403) were clustered into 67 groups utilizing the hierarchical average linkage method available in CATALYST. Subsequently, the highest-ranking

representatives, as judged based on their significance *F*-values (calculated from correlating their fit values against the whole list of collected compounds with the corresponding molecular bioactivities) were selected to represent their corresponding clusters in subsequent QSAR modeling. Table D under Supplementary Materials shows information about representative pharmacophores including their pharmacophoric features, success criteria and differences from corresponding null hypotheses. The table also shows the corresponding Cat. Scramble confidence levels for each representative pharmacophore.

QSAR modeling commenced by selecting a subset of 63 compounds from the total list of inhibitors (**1**–**79**, Table A under Supplementary Materials) as a training set for QSAR modeling; the remaining 16 molecules (ca. 20% of the dataset) were employed as an external test subset for validating the QSAR models. The test molecules were selected as follows: the 79 inhibitors were ranked according to their K_i values, and then every fifth compound was selected for the test set starting from the high-potency end. In this way test molecules represent a range of biological activities similar to that of the training set. The selected test inhibitors are marked with asterisks in table A under Supplementary Materials.

The logarithm of measured $1/K_i$ (μM) values was used in QSAR, thus correlating the data linear to the free energy change. Subsequently, we implemented genetic algorithm and multiple linear regression analyses to select optimal combination of pharmacophoric models and other physicochemical descriptors capable of self-consistent and predictive QSAR model. Section **SM-3** under Supplementary Materials describes extensively the experimental details of QSAR modeling procedure [33,45].

2.1.4. Addition of exclusion volumes

To account for the steric constrains of the binding pocket we decided to decorate the optimal pharmacophore model (i.e., Hypo25/3) with exclusion volumes employing Hip-Hop-Refine module of CATALYST. Hip-Hop-Refine relies on inactive compounds to add exclusion volumes to resemble the steric constrains of the targeted binding site. It identifies regions occupied by the conformers of inactive training compounds and free from active ones. These areas are then filled with excluded volumes [25–27,33]. Subset **VIII** (in Table F under Supplementary Material) was used to construct exclusion spheres around Hyp25/3. Section **SM-4** under Supplementary Materials describes in details the Hip-Hop-Refine algorithm and settings implemented herein to decorate Hypo25/3 with exclusion spheres.

The resulting sterically-refined pharmacophores, as well as their unrefined versions, were validated by receiver operating characteristic curve analyses (ROC) [46–49]. Theoretical and experimental details of this procedure are as shown in Section **SM-5** under Supplementary Material.

2.1.5. In silico screening for new MIF inhibitors

The sterically refined version of Hypo25/3 was employed as 3D search query to screen the 3D flexible molecular database of the National Cancer Institute (NCI). The screening was done employing "Best Flexible Database Search" option implemented within CATALYST. Captured hits were filtered according to Lipinski's [50] and Veber's [49] rules. Remaining hits were fitted against Hypo25/3 and Hypo34/7 using the "best fit" option within CATALYST via implementing equation (D) in Section **SM-2** under Supplementary Materials. The fit values together with the relevant molecular descriptors of each hit were substituted in the optimal QSAR equation. The highest ranking molecules based on QSAR predictions were acquired and tested in vitro.

2.2. In vitro experimental studies

2.2.1. Materials

All of the chemicals used in these experiments were of reagent grade and obtained from commercial suppliers. NCI samples were kindly provided by the national cancer institute.

2.2.2. Quantification of the anti-MIF bioactivities of different hits

MIF tautomerase 96-well plate assay was adapted from standard MIF tautomerase assay as previously described [51]. Briefly, to each well of a 96-well costar plate, 70 μL of 1× phosphate buffered saline (pbs), 10 μL of 10× hit compound stock solution (1000–0.5 μM) or vehicle control, and 20 μL of 10 μg/mL MIF solution were mixed together and incubated for 15 min at room temperature. Then 30 μL of substrate solution (L-3,4–dihydroxyphenylalanine methyl ester and sodium periodate at 6:4 ratio) (made fresh and pre-incubated over 5 min) was added to wells with a multichannel pipette. The plate was shaken for 3 s and immediately read on a kinetic setting (Δoptical density/min) using a Dynatech MR5000 model spectrophotometer every 5 seconds for 10 readings at 470 nm. Results are expressed as % inhibition of control activity (pbs and dmso). Appropriate volume of DMSO is used as negative controls.

3. Results and discussion

We employed HYPOGEN module within CATALYST software package [33] to construct plausible binding hypotheses for a diverse list of MIF inhibitors [34–36,60,61]. Subsequently, genetic function algorithm (GFA) and multiple linear regression (MLR) analyses were employed to search for an optimal QSAR that combine high-quality binding pharmacophore(s) with other molecular descriptors and capable of explaining bioactivity variation across a collection of diverse MIF inhibitors. The optimal pharmacophore was subsequently used as 3D search query to screen the National Cancer Institute (NCI) list of compounds for new MIF inhibitory leads.

CATALYST models drug-receptor interactions using information derived only from the ligands' structures. HYPOGEN identifies a 3D array of a maximum of five chemical features common to active training molecules that provides a relative alignment for each input molecule consistent with their binding to a proposed common receptor site. The training molecules should have activities ranging over approximately four orders of magnitude. The conformational flexibility of training ligands is modeled by creating multiple conformers, sensibly prepared to emphasize representative coverage over a specified energy range.

The chemical features considered by HYPOGEN during pharmacophore modeling can be hydrogen bond donors and acceptors (HBDs and HBAs), aliphatic and aromatic hydrophobes (Hbic), positive and negative ionizable (PosIon and NegIon) groups and aromatic planes (RingArom). The resulting binding hypothesis normally consists of a collection of these features arranged in 3D space. The generated pharmacophore models explain the variability of bioactivities with respect to the geometric localization of the chemical features present in the molecules used to build it. CATALYST pharmacophores have been used as 3D queries for database searching and in 3D-QSAR studies [23–30,40,52].

3.1. Exploration of MIF pharmacophoric space

A total of 79 compounds were used in this study (**1**–**79**, see Table A under supplementary material) [34–36,60,61]. Seven training subsets were selected from the collection. Each subset consisted of inhibitors of wide structural diversity. The biological activity in the training subsets spanned from 3.5 to 4.0 orders of magnitude. The study yielded a total of 560 binding hypotheses for the collected series of MIF inhibitors (see Section 2.1.2 in Section 2 and

Sections **SM-1** and **SM-2** under Supplementary Materials for more details [38,41]).

We decided to explore the pharmacophoric space of MIF inhibitors through 56 HYPOGEN automatic runs and employing seven carefully selected diverse training subsets: subsets **I–VII** in table B under supplementary material. The training compounds in these subsets were of maximal 3D diversity and continuous bioactivity spread over more than 3.5 logarithmic cycles [41]. The software was restricted to explore pharmacophoric models incorporating from zero to one PosIon feature, from zero to three HBA, Hbic, and RingArom features, as shown in Table C under supplementary material. These input features were reasonably selected based on visual evaluation of the training compounds and comparison between the structures of potent, moderate and inactive members. Furthermore, we instructed HYPOGEN to explore only four- and five-featured pharmacophores, i.e., ignore models of lesser number of features in order to further narrow the investigated pharmacophoric space and to signify the feature-rich nature of known MIF ligands (as shown in table C under supplementary material).

In each run, the resulting binding hypotheses were automatically ranked according to their corresponding "total cost" value, which is defined as the sum of error cost, weight cost and configuration cost (see Section 2.1.2 in Section 2 and Section **SM-2** under Supplementary Materials) [33,38–42]. Error cost provides the highest contribution to total cost and it is directly related to the capacity of the particular pharmacophore as 3D-QSAR model, i.e., in correlating the molecular structures to the corresponding biological responses [33,38–42].

HYPOGEN also calculates the cost of the null hypothesis, which presumes that there is no relationship in the data and that experimental activities are normally distributed about their mean. Accordingly, the greater the difference from the null hypothesis cost (i.e., residual cost, table D under Supplementary Materials) the more likely that the hypothesis does not reflect a chance correlation. Additionally, CATALYST implements Fischer's randomization test for additional validation [33,43] (see Section 2.1.2 in Section 2) [33,38–42].

Eventually, 560 pharmacophore models emerged from 56 automatic HYPOGEN runs, out of which only 403 models illustrated Fischer randomization confidence levels ≥85%. These successful models were clustered and the best representatives (67 models, see Section 2.1.3 under Section 2 and table D under Supplementary Materials) were used in subsequent QSAR modeling. Interestingly, the representative models shared comparable features and acceptable statistical success criteria.

Emergence of several statistically comparable pharmacophore models suggests the ability of MIF ligands to assume multiple pharmacophoric binding modes within the binding pocket. Therefore, it is quite challenging to select any particular pharmacophore hypothesis as a sole representative of the binding process.

3.2. QSAR modeling

Despite the excellent value of pharmacophoric hypotheses in probing ligand–macromolecule recognition and as 3D search queries to mine for new biologically interesting scaffolds, their predictive value as 3D-QSAR models is generally hampered by steric shielding and bioactivity modulating auxiliary groups (e.g., electron-donating and withdrawing substitutions) [23–30]. This point combined with the fact that pharmacophore exploration of MIF inhibitors furnished hundreds of binding hypotheses of comparable success criteria prompted us to employ classical QSAR analysis to search for the best combination of pharmacophore(s) and other 2D descriptors capable of explaining bioactivity variation within the collected inhibitors (**1**–**79**, table A under Supplementary Materials). We employed genetic function approximation and multiple linear regression QSAR (GFA-MLR–QSAR) analysis to search for an optimal QSAR equation(s).

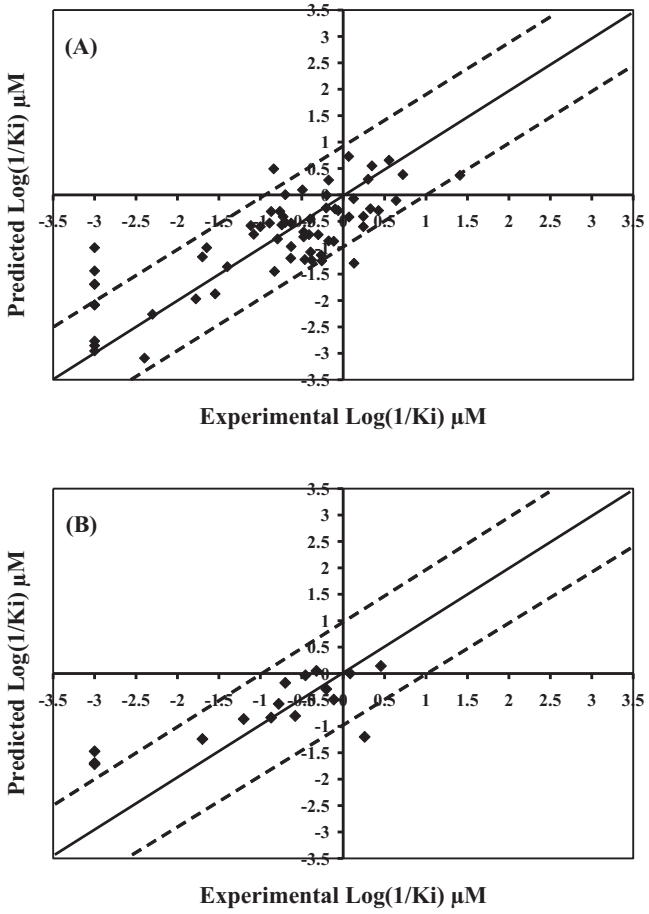

Fig. 1. Experimental versus (A) fitted (63 training compounds, $r^2_{LOO} = 0.748$), and (B) predicted (16 test compounds, $r^2_{PRESS} = 0.619$) bioactivities calculated from the best QSAR model Eq. (2). The solid lines are the regression lines for the fitted and predicted bioactivities of training and test compounds, respectively, whereas the dotted lines indicate 1.0 log point error margins.

The fit values obtained by mapping representative hypotheses (67 models) against collected MIF inhibitors were enrolled, together with around 100 other physicochemical descriptors, as independent variables in GFA-MLR–QSAR analysis (see Section 2.1.3 under Section 2 and Section **SM-3** under Supplementary Materials) [23–30,45,54]. We randomly selected 16 molecules (marked with asterisks in table A under Supplementary Materials) and employed them as external test molecules for validating the QSAR models (r^2_{PRESS}). Moreover, all QSAR models were cross-validated automatically using the leave-one-out cross-validation in CERIUS2 [45,54].

Eq. (2) shows the details of the optimal QSAR model. Fig. 1 shows the corresponding scatter plots of experimental versus estimated bioactivities for the training and testing inhibitors.

$$\log\left(\frac{1}{K_i}\right) = -11.30 + 0.49 \times (\text{dsCH-Count}) + 1.98 \times (\text{NumBonds}) + 1.01 \times (\text{NumTerminalRotomers}) - 0.17 \times (\text{V-ADJ-equ}) + 0.13 \times \left(\text{Hypo25/3}\right) + 0.11 \times (\text{Hypo34/7}) \quad (2)$$

$r_{63} = 0.79$, F-statistic $= 42.8$, $r^2_{LOO} = 0.73$, $r^2_{PRESS(16)} = 0.55$

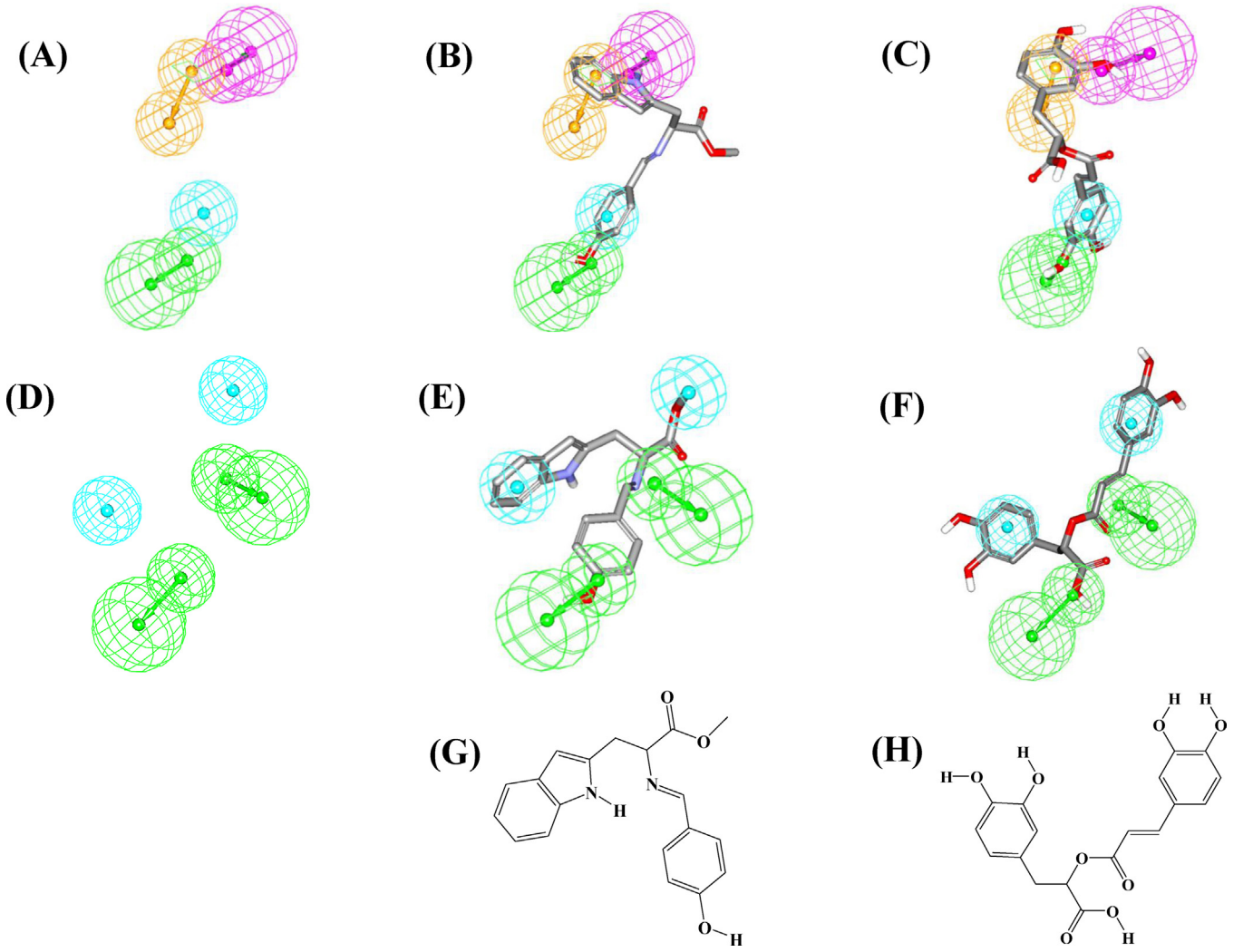

Fig. 2. (A) Pharmacophoric features of Hypo25/3: HBD as pink vectored spheres, Hbic as blue spheres, RingArom as vectored orange spheres, HBA as green vectored spheres, (B) Hypo25/3 fitted against training compound **48** (K_i = 2.4 μM), (C) Hypo25/3 fitted against training compound **70** (K_i = 6.9 μM), (D) pharmacophoric features of Hypo34/7: Hbic as blue spheres, HBA as green vectored spheres, (E) Hypo34/7 fitted against training compound **48**, (F) Hypo34/7 fitted against training compound **70**, (G) Chemical structure of **48**, (H) Chemical Structure of **70**.

where, r_{63} is the correlation coefficient against 63 training compounds, r^2_{LOO} is the leave-one-out correlation coefficient, r^2_{BS} is the bootstrapping regression coefficient and r^2_{PRESS} is the predictive r^2 determined for the 16 test compounds [45,54]. Hypo25/3 and Hypo34/7 represent the fit values of the training compounds against these pharmacophores (shown in Fig. 2) as calculated from equation (D) in Supplementary Materials [33]. dsCH-Count is the count of —CH= fragments in a particular molecule, NumBonds is the number bonds in a particular molecule, NumTerminalRotomers is the number of flexible terminal functional groups. V-ADJ-equ is a complex two-dimensional descriptor related to the number of heavy atoms (vertices) and number of bonds (regardless to their types, also known as edges) [45].

Appearance of NumTerminalRotomers in conjunction with positive regression slope suggests that molecules exhibiting flexible terminal moieties display better affinities to MIF compared to their rigid counterparts. We believe this trend is probably related to entropic binding factors. Although rigid molecules might benefit from tight interactions that yield good enthalpic contacts within the binding pocket, the higher residual mobility of their flexible counterparts (i.e., within the binding pocket) over-compensate the free energy of binding by smaller entropic penalties paid upon binding, which seems to enhance ligand–MIF affinity. Similar entropic contributions into binding have been discussed before [58,59].

On the other hand, the combined emergence of NumBonds and V-ADJ-equ with opposing regression slopes is quite intriguing since NumBonds is an internal component of V-ADJ-equ. However, we believe this behavior encodes for the combined positive contributions of NumBonds and negative effects of the number of ligand's heavy atoms (non-hydrogen atoms, a second component in V-ADJ-equ) in MIF inhibition. This combination is particularly emphasized in aromatic and cyclic structures, i.e., the more cycles the structure includes, the higher the ratio of NumBonds/number of heavy atoms with concomitant increase in observed anti-MIF potency. This trend can be explained based on the fact that MIF's binding site contains 3 aromatic residues, namely, Tyr36, Tyr95, Phe113, which favor π-stacking binding interactions with aromatic ligands. This conclusion is further supported by the emergence of dsCH-Count (refers to number of —CH= fragments) associated with positive regression slope, as seen in Eq. (2).

Emergence of two orthogonal pharmacophoric models, i.e., Hypo25/3 and Hypo34/7 of cross-correlation $r^2 \leq 0.41$ in QSAR Eq. (2) suggests they represent two complementary binding modes

Table 1
Pharmacophoric features and corresponding weights, tolerances and 3D coordinates of Hypo25/3 and Hypo34/7.

Model	Definition		Chemical features						
			HBD		HBA		RingArom		Hbic
Hypo25/3[a]	Weights		1.736		1.736		1.736		1.736
	Tolerances		1.60	2.20	1.60	2.20	1.60	1.60	1.60
	Coordinates	X	6.896	5.625	1.5416	−1.4348	7.1814	4.8459	2.2642
		Y	2.1078	2.2749	−4.8755	−5.0428	2.8906	1.2571	−3.3123
		Z	−1.264	−3.839	2.5400	2.8766	0.9322	1.8688	0.8469

Model	Definition		Chemical features					
			HBA		HBA		Hbic	Hbic
Hypo34/7[b]	Weights		1.95		1.95		1.95	1.95
	Tolerances		1.60	2.20	1.60	2.20	1.60	1.60
	Coordinates	X	4.1049	4.5699	1.618	3.754	−1.0782	−1.02
		Y	1.2656	0.1857	2.124	4.1355	−1.422	4.920
		Z	6.4696	9.2296	1.427	2.0542	5.0932	−0.200

Refined Hypo25/3.
refineXVol1(2.859,−8.217,5.641),refineXVol2(2.859,1.983,4.621),refineXVol3(7.959,−5.157,2.581),refineXVol4(−2.241,−3.117,1.561),refineXVol5 (5.919,6.063,−0.48),refineXVol6(6.939,−8.217,4.621),refineXVol7(4.899,6.063,1.561),refineXVol8(−0.201,−3.117,5.641),refineXVol9(0.819,−0.057,−2.519),refineXVol10 (3.879,−1.077,7.68),refineXVol11(8.979,−3.117,4.621),refineXVol12(9.999,−0.057,−0.479),refineXVol13(3.879,3.003,0.541), refineXVol14(7.959,5.043,6.661),refineXVol15 (8.979,−3.117,1.56),refineXVol16(1.839,−8.217,0.541),refineXVol17(5.919,7.083,5.641), refineXVol18(0.819,−1.077,5.641),refineXVol19(4.899,1.983,−3.539),refineXVol20 (4.899,5.043,−1.499),refineXVol21(0.819,0.963,−1.499),refineXVol22(8.979,−2.097,−2.519),refineXVol23 (11.019,4.023,2.581),refineXVol24(11.019,−1.077,4.621), refine XVol25(1.839,0.963,3.601), refineXVol26(4.899,3.003,3.601),refineXVol27(−1.221,−4.137,−2.519),refineXVol28(1.839,0.963,5.641),refineXVol29(−0.201,−1.077,4.621), refineXVol30(−2.241,−1.077,0.54),refineXVol31 (8.979,−0.057,−3.539),refineXVol32(3.879,−8.217,5.641),refineXVol33(−0.201,−6.177,−2.519),refineXVol34(−0.201, −7.197,4.621),refineXVol35(8.979,−3.117,5.641), refineXVol36 (6.939,3.003,7.681), refineXVol37(7.959,6.063,−0.479), refineXVol38(9.999,1.983,−1.499),refineXVol39 (−1.221,−4.137,4.621),refineXVol40(0.819,−7.197,−0.479),refineXVol41(8.979,−3.117,0.541), refineXVol42(6.939,7.083,1.561),refineXVol43(1.839,1.983,0.541), refine XVol44 (9.999,−2.097,5.641),refineXVol45(−1.221,−1.077,−1.499),refineXVol46(7.959,7.083,5.641),refineXVol47(1.839,0.963,−3.539),refineXVol48(−1.221,−0.057,0.541), refineXVol49(11.019,0.963, 1.561)refineXVol50(9.999,5.043,5.641),refineXVol51(2.859,0.963,6.661),refineXVol52(6.939,−2.097,9.721), refineXVol53(4.899,7.083,3.601), refineXVol54(6.939,−7.197,2.581),refineXVol55(2.859,−2.097,7.681),refineXVol56(8.979,−2.097,−3.539),refineXVol57 (3.879,−3.117,−6.599), refineXVol58(4.899, −8.217,2.581),refineXVol59(−0.201,−0.057,3.601),refineXVol60(−1.221,−1.077,3.601),refineXVol61(6.939,−6.177,1.561), refineXVol62(7.959,−5.157,3.601)refineXV,l63 (−2.241,−5.157,−0.479),refineXVol64(−0.201,−0.057,−0.479),refineXVol65(−0.201,−1.077,−2.519),refineXVol6(−1.221,−3.117,−2.519),refineXVol67(9.999,−1.077, −0.479),refineXVol68(11.019,1.983,1.561),refineXVol69(7.959,−5.157,−2.519), refineXVol70(7.959,0.963,−4.559).

[a] Hypo25/3: the 7th pharmacophore hypothesis generated in the 1st HYPOGEN run (Table D under Supplementary Material).
[b] Hypo34/7: the 8th pharmacophore hypothesis generated in the 8th HYPOGEN run (Table D under Supplementary Material).

accessible to ligands within the binding pocket of MIF. Similar conclusions were reached about the binding pockets of other targets based on QSAR analysis [23–30]. Fig. 2 shows Hypo25/3 and Hypo34/7 and how they map training compounds **48** and **70** (see table A under Supplementary Information). The *X*, *Y*, and *Z* coordinates of the three pharmacophores are illustrated in Table 1.

Interestingly, the regression slopes of the two pharmacophore models suggest they have mediocre but rather equivalent contributions to bioactivity. Nevertheless, both models illustrated reasonable abilities in separating active compounds from inactive decoys in ROC analysis, albeit Hypo25/3 was superior (see **SM-5** under Supplementary Materials for more details) [46–48,56].

Table 2
ROC curve analysis criteria for QSAR-selected pharmacophores and their sterically-refined versions.

Pharmacophore Model	ROC[a]–AUC[b]	ACC[c]	SPC[d]	TPR[e]	FNR[f]
Hypo25/3	0.92	0.97	0.98	0.45	0.015
Hypo34/7	0.83	0.71	0.98	0.06	0.025

[a] ROC: receiver operating characteristic curve.
[b] AUC: area under the curve.
[c] ACC: overall accuracy.
[d] SPC: overall specificity.
[e] TPR: overall true positive rate.
[f] FNR: overall false negative rate.

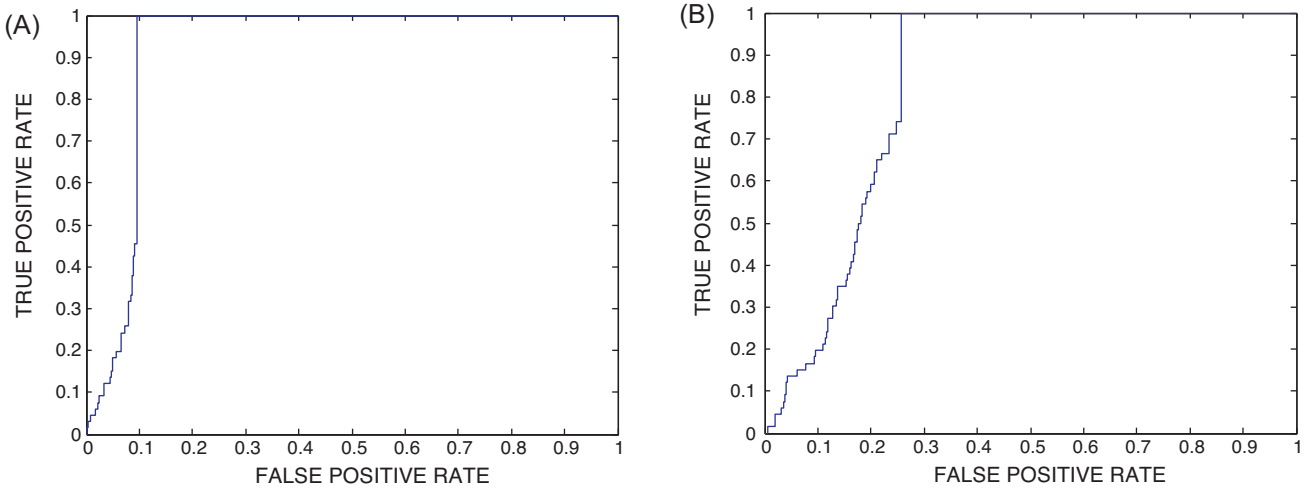

Fig. 3. ROC curves of: (A) Hypo25/3, and (B) Hypo 34/7.

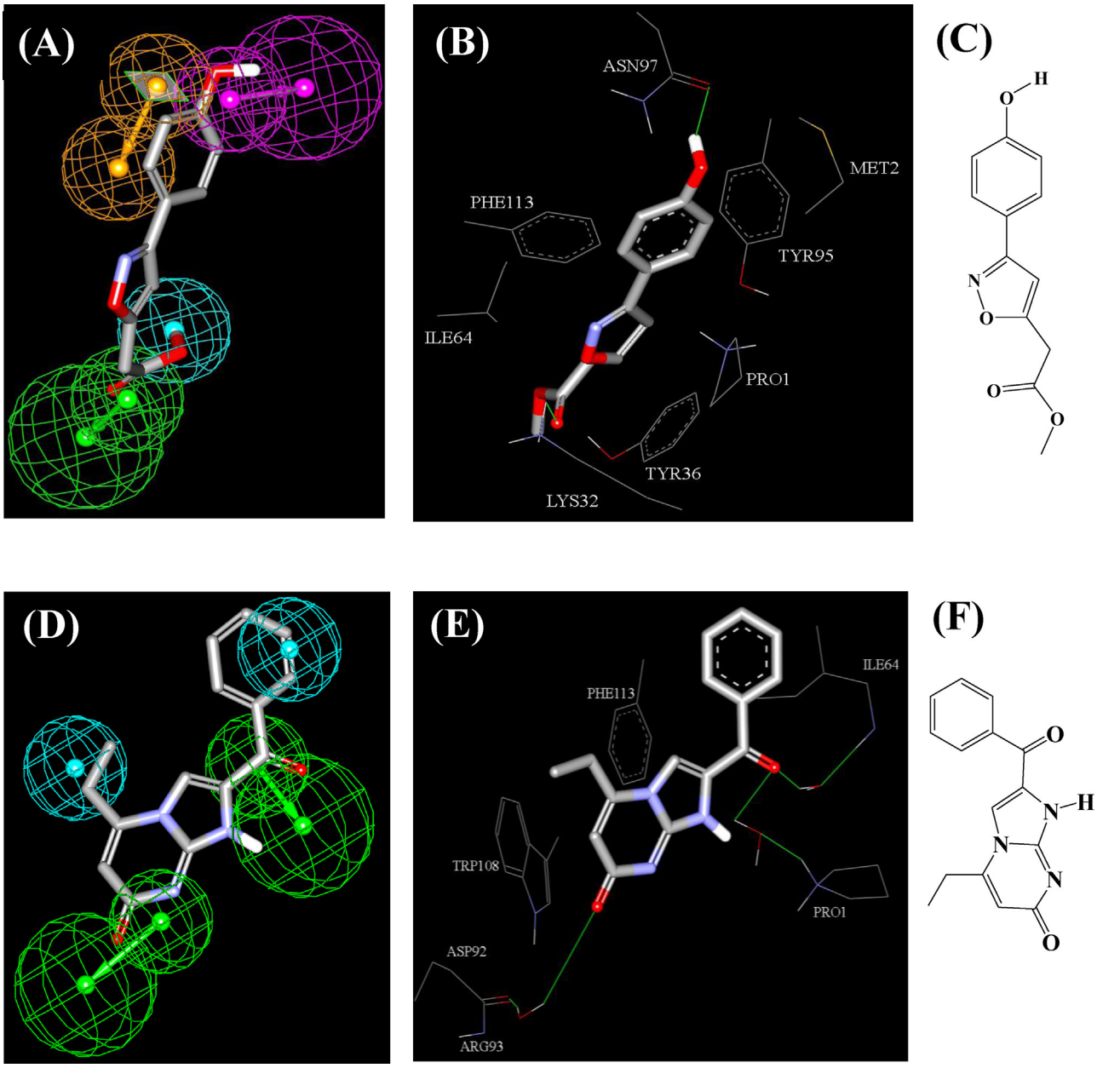

Fig. 4. (A) Mapping of compound **49** (K_i = 5.5 μM, Table A under Supplementary Materials) against Hypo25/3, (B) Co-crystallized complex of **49** within MIF (PDB code: 1LJT, resolution = 2.0 Å), (C) chemical structure of **49**. (D) Mapping of co-crystallized ligand 88X123 (PDB code: 3L5S, resolution = 1.86 Å) against Hypo34/7, (E) Co-crystallized 88X123 into MIF (PDB code: 3L5S, resolution = 1.86 Å), and (F) chemical structure of 88X123.

Table 2 and Fig. 3 show the ROC results of our QSAR-selected pharmacophores.

However, to further understand the significance of the two pharmacophores, we recalculated Eq. (2) without their contributions, as in Eq. (3)

$$\log\left(\frac{1}{K_i}\right) = -9.40 + 0.40 \times (\text{dsCH-Count}) + 1.49 \times (\text{NumBonds}) + 0.77 \times (\text{NumTerminalRotomers}) - 0.119 \times (\text{V-ADJ-equ}) \quad (3)$$

$$r_{63} = 0.71,\ F\text{-statistic} = 15.25,\ r^2_{\text{LOO}} = 0.45,\ r^2_{\text{PRESS(16)}} = 0.48$$

Clearly, the statistical criteria of Eq. (3) are inferior to those of Eq. (2), in particular the predictive r^2_{LOO} suffered from significant drop upon removing the two pharmacophores from the equation.

To correlate the binding features in Hypo25/3 and Hypo34/7 with ligand–receptor binding interactions anchoring inhibitors into MIF's binding pocket, we compared the pharmacophoric features of Hypo25/3 and Hypo34/7 with the way they map two co-crystallized ligands within MIF (PDB codes: 1LJT and 3L5S) [57,13] as in Fig. 4.

Fig. 4A and B compares how training compound **49** (Table A under Supplementary Materials) maps Hypo25/3 with the way it binds within MIF's binding pocket (PDB code: 1LJT). Clearly from the figures, mapping the phenolic hydroxyl of **49** against HBD correspond to hydrogen bonding interaction connecting the same hydroxyl group with the amidic (C=O) side chain of ASN97. Similarly, π-stacking interactions anchoring the phenolic aromatic ring of **49** against the aromatic side chains of Tyr95 and Phe113 seem to be encoded in Hypo25/3 by mapping the same phenolic ring

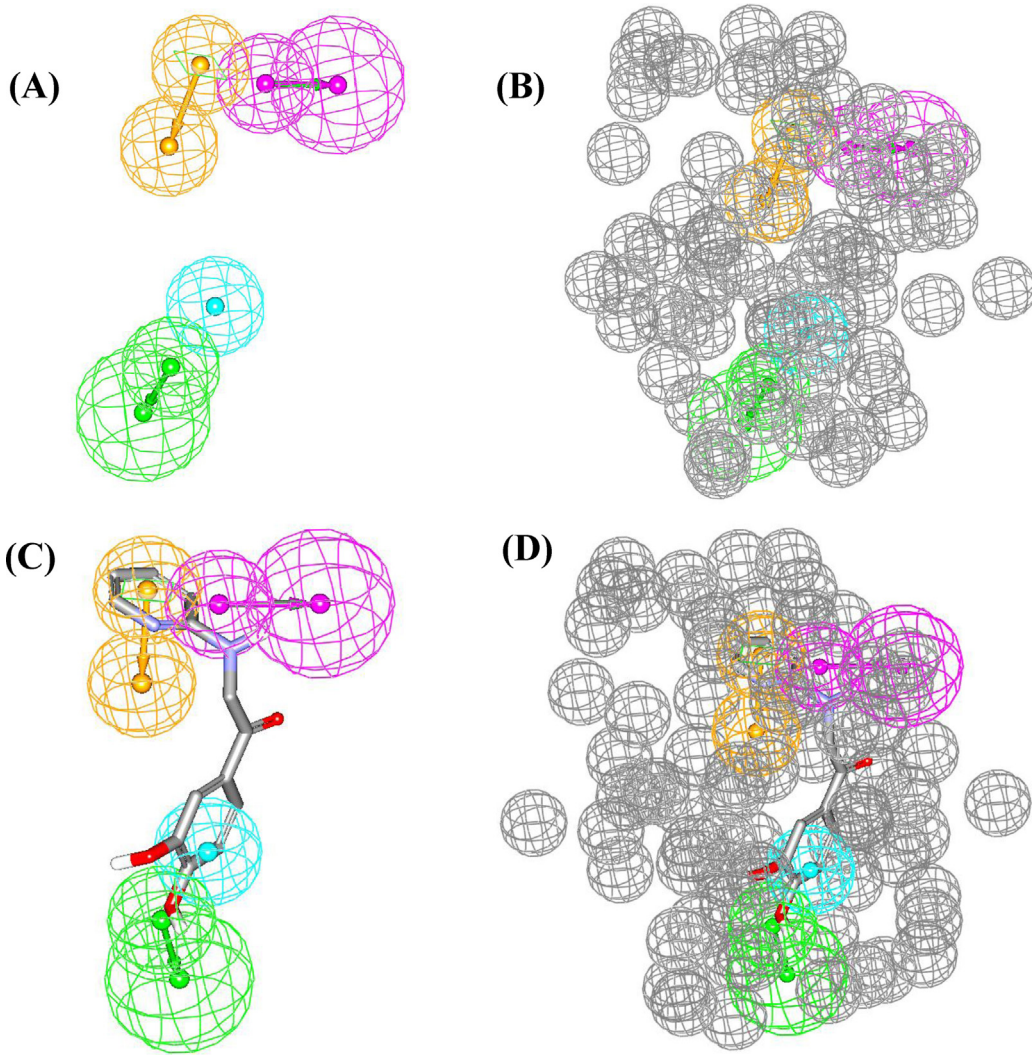

Fig. 5. (A) and (B) show Hypo25/3 without and with steric-refinement, respectively, (C) and (D) show how the two models map hit compound **93** (NCI0082398, Fig. 6).

against RingArom feature. Finally, fitting the terminal methylester of **49** against HBA and Hbic features in Hypo25/3, correlates with hydrogen-bonding and hydrophobic interactions connecting the particular ester carbonyl and methyl groups with the ε-ammonium and isopropyl residues of Lys32 and Ile64, respectively.

On the other hand, Fig. 4D and E compares the co-crystallized pose of ligand 88X123 in MIF (PDB code: 3L5S) with the way it maps Hypo34/7. Mapping the two carbonyl groups of 88X123 against two HBA features in Hypo34/7 correspond to hydrogen-bonding interactions connecting these carbonyls with bridging water molecules tied to the peptidic carbonyl of Arg93, amidic NH of Ile64 and cyclic amine of Pro1. However, fitting the terminal aromatic ring of 88X123 against an Hbic feature in Hypo34/7 agrees with stacking the particular aromatic ring against the isopentyl side chain of Ile64. Similarly, mapping the ethyl substituent of 88X123 against Hbic feature in Hypo34/7 correlates with hydrophobic proximity between this substiuent and the indole ring of Trp108.

Clearly from the above discussion, Hypo25/3 and Hypo34/7 represent two valid binding modes assumed by ligands within MIF.

3.3. *In-silico screening and subsequent in vitro evaluation*

The fact that Hypo25/3 illustrated superior ROC properties, i.e., compared to Hypo34/7 (Table 2 and Fig. 3), prompted us to employ Hypo25/3 as 3D search query against the NCI (238,819 structures) virtual library. However, since pharmacophore models generally fail to define the steric boundaries of corresponding binding pockets, we decided to avoid this liability by complementing Hypo25/3 with exclusion spheres. Lack of steric constrains can render pharmacophoric models rather promiscuous upon use as 3D search queries [29]. We implemented HipHopRefine module of CATALYST to decorate Hypo25/3 with appropriate exclusion spheres (see Section **SM-4** under Supplementary Materials and Section 2.1.4 under Section 2 for more details) [33,55]. We selected a diverse list of training compounds for steric refinement of Hypo25/3 (table E under supplementary material). The training compounds were selected in such away that the bioactivities of weakly active compounds are only explainable by steric clashes within the binding pocket. Fig. 5 shows the sterically refined version of Hypo25/3 and how it maps hit **93** (Table 3 and Fig. 6).

The sterically-refined version of Hypo25/3 captured 1431 compounds from the NCI list of compounds. Subsequent filtering based on Lipinski's and Veber's rules [49,50] yielded 602 compounds. These hits were then fitted against Hypo25/3 (unrefined version) and Hypo34/7, and their fit values, together with other relevant molecular descriptors, were substituted in QSAR Eq. (2) to predict their anti-MIF K_i values. The highest-ranking 61 available hits were evaluated *in vitro* against human MIF via an established assay that measures percent inhibition of MIF tautomerase activity [51]. Table 3 and Fig. 6 show the 10 most active hits,

Table 3
Predicted and experimental bioactivities of high-ranking hit molecules.

Hits[a]	Name[b]	Best fit values against[c]		Predicted K_i (μM)[d]	Experimental %inhibition[e,g]	
		Hypo25/3	Hypo34/7		10 μM	100 μM
83	196539	5.26	5.12	1.48	37 ± 5	58 ± 2
87	668821	5.91	5.28	3.32	14 ± 4	76 ± 3
93	82398	5.04	5.49	3.23	76 ± 4	85 ± 5
99	605767	8.77	5.04	0.97	15 ± 1	80 ± 1
115	174252	5.19	5.34	0.97	5 ± 5	75 ± 7
117	17051	5.68	5.28	0.37	80 ± 1	94 ± 2
118	52107	5.70	5.55	0.57	5 ± 5	40 ± 2
122	164986	5.22	5.73	4.37	5 ± 5	91 ± 2
125	309121	6.22	5.55	4.81	−1 ± 5	40 ± 2
ISO-1	Standard	2.44	7.18	2.3	–	61 ± 5

[a] Chemical structures shown in Fig. 6.
[b] NCI number.
[c] Fit values calculated against respective hypotheses using equation (D) in Supplementary Materials.
[d] predicted K_i according to QSAR Eq. (2).
[e] Experimental inhibition percentages determined at 10 and at 100 μM inhibitor concentrations.
[g] These values represent average results of duplicate measurements ± standard deviation.

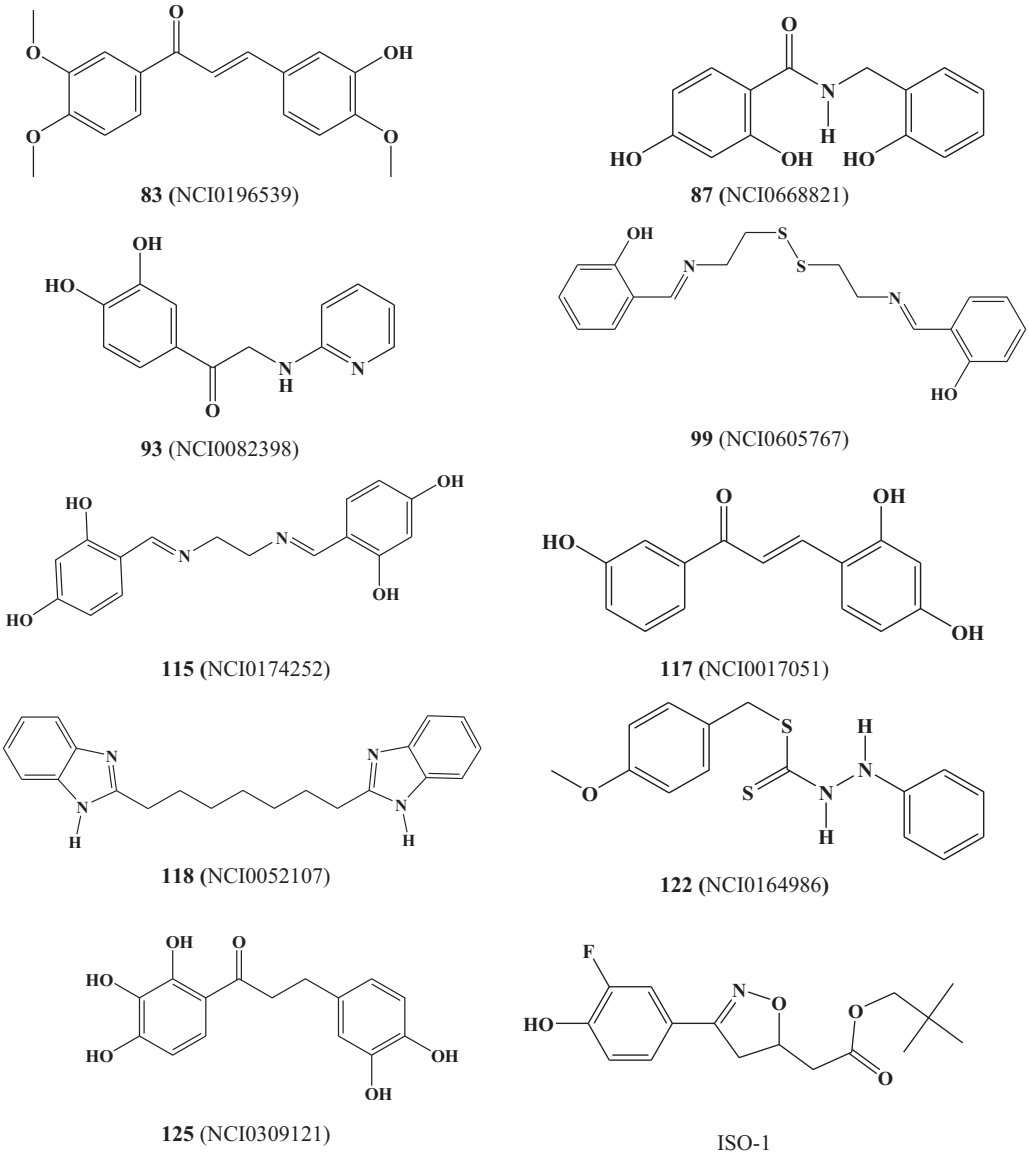

Fig. 6. Chemical structure of the most active hits.

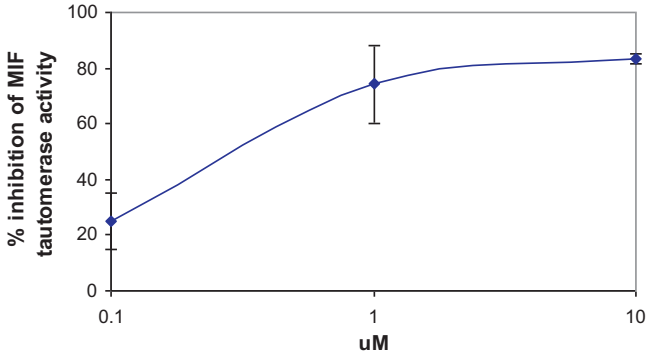

Fig. 7. The dose–response curve of hit compound **93** (NCI0082398).

however, compounds **93** and **117** were the most promising with inhibitory percentages exceeding 85% at 100 μM compared to standard inhibitor **ISO-1**, which gave *ca*. 60% MIF inhibition at similar concentration. Interestingly, both compounds are rather simple and lead-like and can be easily optimized into drug candidates. In particular, compound **93** is quite promising for subsequent optimization, mostly to modify its catechol ring, which is expected to be pharmacokinetically problematic due to its ready oxidation to quinone. Fig. 5 shows how Hypo25/3 fits **93**, while Fig. 7 shows the dose–response curve of **93** with an IC50 value of 270 nM.

4. Conclusions

The pharmacophoric space of MIF inhibitors was explored via seven diverse sets of inhibitors. Genetic algorithm and multiple linear regression analysis were employed to access optimal QSAR model capable of explaining anti-MIF bioactivity variation across 79 MIF inhibitors. Two orthogonal binding hypotheses emerged in the QSAR equation suggesting the existence of at least two distinct binding modes accessible to ligands within MIF binding pocket. The QSAR equation and the associated pharmacophoric models were experimentally validated by the identification of several MIF inhibitors retrieved via *in silico* screening, out of which 10 hits illustrated excellent anti-MIF potencies. Our results suggest that the combination of pharmacophoric exploration and QSAR analyses can be useful tool for finding new diverse MIF inhibitors.

Acknowledgments

The authors thank the Deanship of Scientific Research and Hamdi-Mango Center for Scientific Research at the University of Jordan for their generous funds. The authors are also indebted to the National Cancer Institute for freely providing tested compounds.

Appendix A. Supplementary data

Supplementary data associated with this article can be found, in the online version, at http://dx.doi.org/10.1016/j.jmgm.2013.03.003.

References

[1] J.A. Baugh, R. Bucala, Macrophage migration inhibitory factor, Critical Care Medicine 30 (2002) S27–S35.
[2] J. Bernhagen, T. Calandra, R.A. Mitchell, S.B. Martin, K.J. Tracey, W. Voelter, K.R. Manogue, A. Cerami, R. Bucala, MIF is a pituitary-derived cytokine that potentiates lethal endotoxemia, Nature 365 (1993) 756–759.
[3] B. Bloom, B. Bennett, Mechanism of a reaction in vitro associated with delayed-type hypersensitivity, Science 153 (1966) 80–82.
[4] N. Petrovsky, L. Socha, D. Silva, A.B. Grossman, C. Metz, R. Bucala, Macrophage migration inhibitory factor exhibits a pronounced circadian rhythm relevant to its role as a glucocorticoid counter-regulator, Immunology and Cell Biology 81 (2003) 137–143.
[5] S.C. Donnelly, R. Bucala, Macrophage migration inhibitory factor: a regulator of glucocorticoid activity with a critical role in inflammatory disease, Molecular Medicine Today 3 (1997) 502–507.
[6] E. Rosengren, R. Bucala, P. Aman, L. Jacobsson, G. Odh, C.N. Metz, H. Rorsman, The immunoregulatory mediator macrophage migration inhibitory factor (MIF) catalyzes a tautomerization reaction, Molecular Medicine 2 (1996) 143–149.
[7] R.A. Mitchell, R. Bucala, Tumor growth-promoting properties of macrophage migration inhibitory factor (MIF), Seminars in Cancer Biology 10 (2000) 359–366.
[8] T. Hagemann, S.C. Robinson, R.G. Thompson, K. Charles, H. Kulbe, F.R. Balkwill, Ovarian cancer cell-derived migration inhibitory factor enhances tumor growth, progression, and angiogenesis, Molecular Cancer Therapeutics 6 (2007) 1993–2002.
[9] A. Mikulowska, C.N. Metz, R. Bucala, R. Holmdahl, Macrophage migration inhibitory factor is involved in the pathogenesis of collagen type II-induced arthritis in mice, Journal of Immunology 158 (1997) 5514–5517.
[10] L.R. McLean, Y. Zhang, H. Li, Y.-M. Choi, Z. Han, R.J. Vaz, Y. Li, Fragment screening of inhibitors for MIF tautomerase reveals a cryptic surface binding site, Bioorganic and Medicinal Chemistry Letters 20 (2010) 1821–1824.
[11] M. Orita, S. Yamamoto, N. Katayama, S. Fujita, Macrophage migration inhibitory factor and the discovery of tautomerase inhibitors, Current Pharmaceutical Design 8 (2002) 1297–1317.
[12] M. Orita, S. Yamamoto, N. Katayama, M. Aoki, K. Takayama, Y. Yamagiwa, N. Seki, H. Suzuki, H. Kurihara, H. Sakashita, M. Takeuchi, S. Fujita, T. Yamada, A. Tanaka, Coumarin and chromen-4-one analogues as tautomerase inhibitors of macrophage migration inhibitory factor: discovery and X-ray crystallography, Journal of Medicinal Chemistry 44 (2001) 540–547.
[13] L.R. McLean, Y. Zhang, H. Li, Y.M. Choi, Z. Han, R.J. Vaz, Y. Li, Fragment screening of inhibitors for MIF tautomerase reveals a cryptic surface binding site, Bioorganic and Medicinal Chemistry Letters 20 (2010) 1821–1824.
[14] F. El Turk, B. Fauvet, H.O. -Sakouhi, A. Lugari, S. Betzi, P. Roche, X. Morelli, H.A. Lashuel, An integrative in silico methodology for the identification of modulators of macrophage migration inhibitory factor (MIF) tautomerase activity, Bioorganic and Medicinal Chemistry 18 (2010) 5425–5440.
[15] Y. Fukunishi, Structure-based drug screening and ligand-based drug screening with machine learning, Combinatorial Chemistry & High Throughput Screening 12 (2009) 397–408.
[16] J. Garai, V. Molnár, D. Erős, L. Őrfi, T. Lóránd, MIF tautomerase inhibitor potency of α,β-unsaturated cyclic ketones, International Immunopharmacology 7 (2007) 1741–1746.
[17] R.A. Beeley, N.C. Sage, GPCRs: an update on structural approaches to drug discovery, Targets 2 (2003) 19–25.
[18] G. Klebe, Virtual ligand screening: strategies, perspectives and limitations, Drug Discovery Today 11 (2006) 580–594.
[19] H. Steuber, M. Zentgraf, C. Gerlach, C.A. Sotriffer, A. Heine, G.J. Klebe, Expect the unexpected or caveat for drug designers: multiple structure determinations using aldose reductase crystals treated under varying soaking and co-crystallisation conditions, Molecular Biology 363 (2006) 174–187.
[20] M.T. Stubbs, S. Reyda, F. Dullweber, M. Moller, G. Klebe, D. Dorsch, W. Mederski, H. Wurziger, pH-Dependent binding modes observed in trypsin crystals: lessons for structure-based drug design, ChemBioChem 3 (2002) 246–249.
[21] M.A. DePristo, P.I.W. de Bakker, T.L. Blundell, Heterogeneity and inaccuracy in protein structures solved by X-ray crystallography, Structure 12 (2004) 831–838.
[22] F. El-Turk, M. Cascella, H.O. -Sakouhi, R.L. Narayanan, L. Leng, R. Bucala, M. Zweckstetter, U. Rothlisberger, H.A. Lashuel, The conformational flexibility of the carboxy terminal residues 105–114 is a key modulator of the catalytic activity and stability of macrophage migration inhibitory factor, Biochemistry 47 (2008) 10740–10756.
[23] M.O. Taha, Y. Bustanji, M.A.S. Al-Ghussein, M. Mohammad, H. Zalloum, I.M. Al-Masri, N. Atallah, Pharmacophore modeling, quantitative structure-activity relationship analysis and in silico screening reveal potent glycogen synthase kinase-3β inhibitory activities for cimetidine, hydroxychloroquine and gemifloxacin, Journal of Medicinal Chemistry 51 (2008) 2062–2077.
[24] M.O. Taha, N. Atallah, A.G. Al-Bakri, C. Paradis-Bleau, H. Zalloum, K. Younis, R.C. Levesque, Discovery of new MurF inhibitors via pharmacophore modeling and QSAR analysis followed by in-silico screening, Bioorganic and Medicinal Chemistry 16 (2008) 1218–1235.
[25] M.O. Taha, Y. Bustanji, A.G. Al-Bakri, M. Yousef, W.A. Zalloum, I.M. Al-Masri, N. Atallah, Discovery of new potent human protein tyrosine phosphatase inhibitors via pharmacophore and QSAR analysis followed by in silico screening, Journal of Molecular Graphics and Modelling 25 (2007) 870–884.
[26] I.M. Al-masri, M.K. Mohammad, M.O. Taha, Discovery of DPP IV inhibitors by pharmacophore modeling and QSAR analysis followed by in silico screening, ChemMedChem 3 (2008) 1763–1779.
[27] M.O. Taha, L.A. Dahabiyeh, Y. Bustanji, H. Zalloum, S. Saleh, Combining ligand-based pharmacophore modeling, QSAR analysis and in-silico screening for the discovery of new potent hormone sensitive lipase inhibitors, Journal of Medicinal Chemistry 51 (2008) 6478–6494.
[28] A. Al-Nadaf, G. Abu Sheikha, M.O. Taha, Elaborate ligand-based pharmacophore exploration and QSAR analysis guide the synthesis of novel pyridinium-based potent β-secretase inhibitory leads, Bioorganic and Medicinal Chemistry 18 (2010) 3088–3115.

[29] A.M. Abu-Hammad, M.O. Taha, Pharmacophore modeling, quantitative structure–activity relationship analysis, and shape-complemented in silico screening allow access to novel influenza neuraminidase inhibitors, Journal of Chemical Information and Modeling 49 (2009) 978–996.
[30] R. Abu Khalaf, G. Abu Sheikha, Y. Bustanji, M.O. Taha, Discovery of new cholesteryl ester transfer protein inhibitors via ligand-based pharmacophore modeling and QSAR analysis followed by synthetic exploration, European Journal of Medical Chemistry 45 (2010) 1598–1617.
[31] M.A. Al-Sha'er, M.O. Taha, Discovery of novel CDK1 inhibitors by combining pharmacophore modeling, QSAR analysis and in silico screening followed by in vitro bioassay, European Journal of Medical Chemistry 45 (2010) 4316–4330.
[32] M.A. Al-Sha'er, M.O. Taha, Elaborate ligand-based modeling reveals new nanomolar heat shock protein 90α inhibitors, Journal of Chemical Information and Modeling 50 (2010) 1706–1723.
[33] CATALYST 4.11 Users' Manual, Accelrys Software Inc., San Diego, CA, 2005.
[34] H.O. -Sakouhi, F. El-Turk, B. Fauvet, M.-K. Cho, D.P. Karpinar, D.L. Roy, M. Dewor, T. Roger, J. Bernhagen, T. Calandra, M. Zweckstetter, H.A. Lashuel, Identification and characterization of novel classes of macrophage migration inhibitory factor (MIF) inhibitors with distinct mechanisms of action, Journal of Biological Chemistry 285 (2010) 26581–26598.
[35] J. Garai1, T. Lóránd, Macrophage migration inhibitory factor (MIF) tautomerase inhibitors as potential novel anti-inflammatory agents: current developments, Current Medicinal Chemistry 16 (2009) 1091–1114.
[36] N.M. Dagia, D.V. Kamath, P. Bhatt, R.D. Gupte, S.S. Dadarkar, L.F.G. Agarwal, A. Chetrapal-Kunwar, S. Balachandran, S. Srinivasan, J. Bose, K. Pari, C. B-Rao, S.S. Parkale, P.K. Gadekar, A.H. Rodge, N. Mandrekar, R.A. Vishwakarma, S. Sharma, A fluorinated analog of ISO-1 blocks the recognition and biological function of MIF and is orally efficacious in a murine model of colitis, European Journal of Pharmacology 607 (2009) 201–212.
[37] Y. Cheng, W. Prusoff, Relationship between the inhibition constant (K_i) and the concentration of inhibitor which causes 50 percent inhibition (I50) of an enzymatic reaction, Biochemical Pharmacology 22 (1973) 3099–3108.
[38] J. Sutter, O. Güner, R. Hoffmann, H. Li, M. Waldman, in: O.F. Güner (Ed.), Pharmacophore Perception, Development, and Use in Drug Design, International University Line, La Jolla, CA, 2000, pp. 501–511.
[39] Y. Kurogi, O.F. Güner, Pharmacophore modeling and three dimensional database searching for drug design using catalyst, Current Medicinal Chemistry 8 (2001) 1035–1055.
[40] K. Poptodorov, T. Luu, T. Langer, R. Hoffmann, in: R.D. Hoffmann (Ed.), Methods and Principles in Medicinal Chemistry. Pharmacophores and Pharmacophores Searches;, vol. 2, Wiley-VCH, Weinheim, Germany, 2006, pp. 17–47.
[41] H. Li, J. Sutter, R. Hoffmann, in: O.F. Güner (Ed.), Pharmacophore Perception, Development, and Use in Drug Design, International University Line, La Jolla, CA, 2000, pp. 173–189.
[42] I.B. Bersuker, S. Bahçeci, J.E. Boggs, in: O.F. Güner (Ed.), Pharmacophore Perception, Development, and Use in Drug Design, International University Line, La Jolla, CA, 2000, pp. 457–473.
[43] R. Fischer, The Principle of Experimentation Illustrated by a Psycho-Physical ExpeHafner Publishing Co., 8th ed., Hafner Publishing, New York, 1966 (chapter II).
[44] CERIUS2 LigandFit User Manual (version 4.10), Accelrys Inc., San Diego, CA (2005) 3–48.
[45] CERIUS2, QSAR Users' Manual, version 4.10, Accelrys Inc., San Diego, CA (2005) 43–88, 221–235, 237–250.
[46] J. Kirchmair, P. Markt, S. Distinto, G. Wolber, T. Langer, Evaluation of the performance of 3D virtual screening protocols: RMSD comparisons, enrichment assessments, and decoy selection—What can we learn from earlier mistakes? Journal of Computer-Aided Molecular Design 22 (2008) 213–228.
[47] J.J. Irwin, B.K. Shoichet, ZINC – a free database of commercially available compounds for virtual screening, Journal of Chemical Information and Computer Science 45 (2005) 177–182.
[48] N. Triballeau, F. Acher, I. Brabet, J.-P. Pin, H.-O. Bertrand, Virtual screening workflow development guided by the "receiver operating characteristic" curve approach, application to high-throughput docking on metabotropic glutamate receptor subtype 4, Journal of Medicinal Chemistry 48 (2005) 2534–2547.
[49] D.F. Veber, S.R. Johnson, H.Y. Cheng, B.R. Smith, K.W. Ward, K.D. Kopple, Molecular properties that influence the oral bioavailability of drug candidates, Journal of Medicinal Chemistry 45 (2002) 2615–2623.
[50] C.A. Lipinski, F. Lombardo, B.W. Dominy, P.J. Feeney, Experimental and computational approaches to estimate solubility and permeability in drug discovery and development settings, Advanced Drug Delivery Reviews 46 (2001) 3–26.
[51] A. Dios, R.A. Mitchell, B. Aljabari, J. Lubetsky, K. O'Connor, H. Liao, P.D. Senter, K.R. Manogue, E. Lolis, C. Metz, R. Bucala, D.J. Callaway, Y. Al-Abed, Journal of Medicinal Chemistry 45 (2002) 2410–2416.
[52] J.H. Van Drie, Pharmacophore discovery—lessons learned, Current Pharmaceutical Design 9 (2003) 1649–1664.
[53] R.P. Sheridan, S.K. Kearsley, Why do we need so many chemical similarity search methods? Drug Discovery Today 7 (2002) 903–911.
[54] L.F. Ramsey, W.D. Schafer, The Statistical Sleuth, 1st ed., Wadsworth Publishing Company, Belmont, CA, 1997.
[55] O.O. Clement, A.T. Mehl, in: O.F. Guner (Ed.), Pharmacophore perception, development, and use in drug design. IUL Biotechnology Series, International University Line, La Jolla, CA, 2000, pp. 71–84.
[56] M.L. Verdonk, L. Marcel, V. Berdini, M.J. Hartshorn, W.T.M. Mooij, C.W. Murray, R.D. Taylor, P. Watson, Virtual screening using protein-ligand docking: avoiding artificial enrichment, Journal of Chemical Information and Computer Science 44 (2004) 793–806.
[57] J.B. Lubetsky, A. Dios, J. Han, B. Aljabari, B. Ruzsicska, R. Mitchell, E. Lolis, Y. Al-Abed, The tautomerase active site of macrophage migration inhibitory factor is a potential target for discovery of novel anti-inflammatory agents, Journal of Biological Chemistry 277 (2002) 24976–32482.
[58] C. Gerlach, M. Smolinski, H. Steuber, C.A. Sotriffer, A. Heine, D.G. Hangauer, G. Klebe, Thermodynamic inhibition profile of a cyclopentyl and a cyclohexyl derivative towards thrombin: the same but for different reasons, Angewandte Chemie International Edition 46 (2007) 8511–8514.
[59] A.M. Davis, S.A. St-Gallay, G.J. Kleywegt, Limitations and lessons in the use of X-ray structural information in drug design, Drug Discovery Today 13 (2008) 831–841.
[60] P.D. Senter, Y. Al-Abed, C.N. Metz, F. Benigni, R.A. Mitchell, J. Chesney, J. Han, C.G. Gartner, S.D. Nelson, G.J. Todaro, R. Bucala, Inhibition of macrophage migration inhibitory factor (MIF) tautomerase and biological activities by acetaminophen metabolites, PNAS 99 (2002) 144–149.
[61] K.F. Cheng, Y. Al-Abed, Critical modifications of the ISO-1 scaffold improve its potent inhibition of macrophage migration inhibitory factor (MIF) tautomerase activity, Bioorganic and Medicinal Chemistry Letters 16 (2006) 3376–3379.
[62] L.G. Warren, D.T. Do, P.B. Kelley, A. Nicholls, D.S. Warren, Essential considerations for using protein–ligand structures in drug discovery, Drug Discovery Today 17 (2012) 1270–2128.
[63] Z. Cournia, L. Leng, S. Gandavadi, X. Du, R. Bucala, W.L. Jorgensen, Discovery of human macrophage migration inhibitory factor (MIF)-CD74 antagonists via virtual screening, Journal of Medicinal Chemistry 52 (2009) 416–424.
[64] M. Winner, J. Meier, S. Zierow, B.E. Rendon, G. Chrichlow, R. Riggs, R. Bucala, L. Leng, N. Smith, E. Lolis, J.O. Trent, R.A. Mitchell, A novel, macrophage migration inhibitory factor suicide substrate inhibits motility and growth of lung cancer cells, Cancer Research 68 (2008) 7253–7257.
[65] T.A. Soares, R.D. Lins, T.P. Straatsma, J.M. Briggs, Internal dynamics and ionization states of the macrophage migration inhibitory factor: comparison between wild-type and mutant forms, Biopolymers 65 (2002) 313–323.
[66] L. Xu, Y. Li, L. Li, S. Zhou, T. Hou, Understanding microscopic binding of macrophage migration inhibitory factor with phenolic hydrazones by molecular docking, molecular dynamics simulations and free energy calculations, Molecular BioSystems 8 (2012) 2260–2273.